Full Title:

Remote Weather Associated with South Pacific Subtropical Sea Level High Properties

Short Title:

Remote Weather Associated with the South Pacific Subtropical High

Richard Grotjahn
Dept. of Land, Air, and Water Resources,
University of California, Davis CA 95616 USA
email: grotjahn@ucdavis.edu
phone: 530 752-2246
fax: 530 752-1793

Accepted for publication in:
International Journal of Climatology

August 2003
Revised: December 2003

ABSTRACT

The subtropical highs in sea level pressure (SLP) are little-studied and incompletely understood. In recent years, three groups of theories, tropical divergent circulations, subtropical Rossby wavetrains, and midlatitude frontal cyclone interactions, have been proposed for remote maintenance of these highs. The latter is presented here as a remote forcing of these highs for the first time in the reviewed literature. The focus of the study is upon illuminating associations between these mechanisms and the South Pacific subtropical high in sea level pressure (SP high). Precipitation, outgoing longwave radiation, velocity potential, and divergent winds are used as proxy markers for the remote forcing mechanisms. The tools used include composites, one-point correlations, autocorrelations, cross-correlations, and cross spectra. Observational evidence, in monthly and daily data is examined that appears to support each mechanism. Associations seen in monthly data are better understood in daily data at various lags. Convection over Amazonia, coordinated with suppressed convection in the western tropical Pacific lead to enhanced SLP on the tropical side of the high. Midlatitude weather systems are the strongest influence upon the maximum SLP and SLP on the higher latitude side of the high. The western side is associated with both middle and lower latitude phenomena, such as the south Pacific convergence zone. Various properties of the high have a strong period around 45 days. Associations to the Madden-Julian oscillation (MJO) and “El Nino Southern Oscillation” (ENSO) are explored and are strong only for the tropical side of the SP high.

KEY WORDS: Pacific, subtropical highs, correlations, composites, SLP, ENSO, MJO

1. INTRODUCTION

The subtropical highs lie in a transition region between the tropics, dominated by convection, and the middle latitudes, dominated by frontal cyclones. The maintenance of these highs and their effects upon adjacent regions have received surprisingly little study. The subject is ripe for study now that the satellite era exceeds two dozen years and now that excellent datasets are becoming available (e.g. the NCEP/NCAR reanalysis data, Kistler et al., 2001).

Climatologically, the North Pacific (NP) high expands greatly during spring and shrinks during fall. In the South Pacific a corresponding subtropical high (hereafter the SP high) undergoes a smaller amplitude seasonal cycle but with a different seasonal phase (peaking in Spring). Figure 1 shows the means, medians, and first and third quartiles by month. The NP high has a prominent peak at July. The SP high has a broader peak over the September through November period. The reasons for the differing seasonal changes are unclear, but are likely linked to forcing by remote events and processes. Climatological information has appeared in papers such as: Taljaard (1967), Jones and Simmonds (1994), Leighton (1994), Sinclair (1996) and references therein.

The remote forcing mechanisms proposed to date settle into three general categories: 1) thermally direct tropical circulations, 2) tropical convection that forces a Rossby wavetrain, and 3) interactions with midlatitude frontal cyclones. Some details of these mechanisms are provided in a later section. These mechanisms provide a framework for understanding the associations. The focus of this report is upon observed associations, not upon evaluating proposed mechanisms. However, the first two mechanisms would benefit from further observational analysis. And, the third has (apparently) been unrecognized except in work by the author reported at scientific conferences.

This report summarizes some data analysis of monthly and daily data for the SP high. In addition, some analysis of the NP high will be included when it contrasts with the SP high results.

2. THREE REMOTE FORCING MECHANISMS

2.1 thermally direct tropical circulations

This mechanism extends the typical discussion of *zonal mean* fields that can be found in textbooks (e.g. Grotjahn, 1993). The argument proceeds like this: strong latent heating in the intertropical convergence zone (hereafter, ICZ) along with diabatic cooling in the subtropics drives a thermally direct circulation. On the zonal mean, a divergent circulation is set up, commonly labeled the "Hadley" cell. A sea level pressure (hereafter: SLP) pattern to sustain these ageostrophic motions has a subtropical high and an ICZ trough. This mechanism is emphasized in Chen et al. (2001).

When viewed in the longitudinal direction, the meridional component of the motion is acted upon by Coriolis and pressure forces, thereby generating zonal accelerations. Due to boundary layer friction (so the argument goes) the surface easterly component is much smaller at the ICZ than the upper westerly component above the subtropical high; thus, rising and subsequent sinking occur at different longitudes. Sinking occurs where there is diabatic cooling. Extending this view to recognize that tropical convection has significant zonal variation (and the oceanic preference for low level cooling) yields the observed pattern of subtropical highs East (and poleward) of the peak diabatic heating. Divergent circulations generated by the Asian monsoon have an east-west component (the "Walker" circulation) that would also help enhance the NP high. Trenberth and Shea (1987) show a sizeable anti-correlation between SLP at Darwin, Australia and (opposite) SLP changes over a broad area encompassing much of the tropical sides of the NP and SP highs. This mechanism would assign a secondary role to convection over northern South America and Central America during boreal summer for the NP high because the areal extent and other properties are greater for the SE Asian

monsoon. For the SP high the issue is less clear because the properties of convection over Amazonia are more comparable to those over the south Pacific convergence zone (hereafter: SPCZ). The time mean divergent flows from the SPCZ and from Amazonia have similar strength at 200 hPa over the southeastern Pacific.

This view invokes the intuition of following parcels as they traverse a thermally direct cell. So, when one looks at maps of 200 hPa divergent winds one might follow those winds to connect areas of convection with downstream sinking regions. Doing so finds that divergent winds generated by the Asian Monsoon dwarf the divergent flow from Central American convection over the North Pacific. However, parcels might not have to complete such "closed" circuits according to the next mechanism.

2.2 Rossby wavetrain from tropical heat source

In the first of a series of papers, Hoskins (1996) connects the subtropical high to latent heating released to the *east* and equatorward of the high. He interprets his results by analogy to works of Gill (Gill, 1980; Heckley and Gill, 1984; etc.). The main idea is that the tropical heating sets up a stationary Rossby wavetrain with a surface low to the east and poleward of the heating. Sinking is presumed to occur on the west side of the low. The divergence term (f*dw/dz) and the planetary vorticity advection term (β*v) in the vorticity equation are assumed to balance approximately implying equatorward flow beneath the maximum in downward motion. These papers emphasize that such winds could lie on the east side of the subtropical high.

Hoskins and collaborators use atmospheric general circulation models (AGCMs) to test factors that may affect the highs. Hoskins and Rodwell (1995) discuss experiments testing mountains versus no mountains, heating versus no heating, and various "linear" versus nonlinear integrations. They study the June-August season. The heating is global in extent and based upon observed residuals in a potential temperature conservation equation. Cooling over both Pacific highs and heating over Central America, as well as strong Asian monsoon heating are sufficient to generate NP and SP highs in their model

runs. Topography improves the fidelity of the highs (the SP high is specifically mentioned) but they write that topography cannot create the highs alone. Their linear and nonlinear results for heating are similar. Hoskins et al. (1999) interpret their figure 3 as linking Central American summer convection with the NP high. They comment that enhanced cooling in the region of the NP high improves the simulation and that: "…ICZ region heating is also helpful in increasing the realism." The last comment blurs the distinction between this mechanism and the divergent circulation mechanism. Shaffrey et al (2002) investigate the sensitivity of the NP high to mountains, albedo, and precipitation, all to the East, yet they do not show maps of the SLP response. Instead, they emphasize vertical velocity and meridional wind response. Shaffrey et al. (2002) also write that they expect "midlatitude westerlies descend … not the upper tropospheric easterlies associated with the upper level [North American summer] monsoon circulation".

In all of the works by Hoskins and his collaborators prior to 2002, frontal cyclones were intentionally excluded from their study by terminating AGCM calculations started from rest after no more than 20 days. Shaffrey et al. (2002) consider seasonal runs of an AGCM that presumably allows frontal cyclones, but they still ignore frontal cyclones in their report. Frontal cyclones drive a third proposed remote mechanism.

2.3 interactions with midlatitude frontal cyclones

The zonal mean subtropical highs lie at the interface between the tropics and midlatitudes so one would expect these highs to respond to weather not just from the tropics but also from higher latitudes. Large scale weather in midlatitudes is dominated by frontal cyclones. To the author's knowledge, this report is the first refereed publication in which frontal cyclones are advanced as a remote forcing mechanism (though only in a qualitative way). To initiate discussion of this proposed mechanism, it is well known that midlatitude eddies strongly affect zonal mean momentum and heat transport in middle and high latitudes. Observations (e.g. Oort and Peixoto, 1983) show that transient eddies account for a significant fraction of these fluxes in the *subtropics* as

well. When input into zonal mean models, like the "Kuo-Eliassen" equation (e.g. Pfeffer, 1981) transient midlatitude eddy fluxes are a significant driving mechanism for the zonal mean Hadley cells. The divergent circulation of such a model supports a zonal mean subtropical high.

Some evidence associating midlatitude weather with subtropical highs is indirect. Wallace (1983) notes that the (mid-tropospheric) subtropical stationary wave "is at least partially forced from higher latitudes" as judged from robust, observed Eliassen-Palm (EP) fluxes. Divergent circulations around developing, mature, and decaying frontal cyclones may communicate the cyclone forcing to the subtropical high. Meridional motions are expected from thermal wind balance as well as part of the cyclone energetics (e.g. Grotjahn, 1993; Holton, 1992) and have long been noticed in data (e.g. Blackmon, et al., 1977). The associated sinking is generally over an adjacent high that can occur at a lower latitude. In addition, there are divergent circulations associated with jet streaks (e.g. Carlson, 1994) specifically, sinking in the right jet exit region (Northern Hemisphere) that may reinforce the high. Qualitative evidence is drawn from sequences of daily synoptic charts over the North Pacific; one often sees large deformations in the subtropical high associated with the passage of frontal cyclones. Also, highs originating at higher latitudes seem to merge with and strengthen the subtropical high.

3. DATA AND ANALYSIS METHODS

NCEP/NCAR reanalysis data (see Kalnay, et al., 1996; Kistler et al., 2001) provided by the Climate Diagnostics Center (CDC) of NOAA are used for this study. Only data supplemented by satellite measurements are used, starting with January 1979. Some results shown here were presented *orally* at several conferences in recent years. Monthly data were shown at the 6th conference on Southern Hemisphere Meteorology and Oceanography (Grotjahn, 2000) and 13th conference on Atmospheric and Oceanic Fluid Dynamics (Grotjahn and Immel, 2001). Daily data results were shown at the 7th conference on Southern Hemisphere Meteorology and Oceanography (Grotjahn, 2003). However, the figures here have not been reproduced elsewhere in print.

Figure 1 shows a broad maximum in the SP high central pressure over summer months of December-February but also the spring months of October and November. Since *other* regions and fields have a strong trend during the spring, monthly anomaly (MA) data were generated in order to remove that trend and to isolate variations between months. Allowing months adjacent to the 3-month summer season also increases the sample size. For the SP high, the months October through February were used in MA data. The SP high tends to be stronger during these months. The procedure is simply to average all the occurrences of a specific month in the data record used (1979-2001, say) and then create the MA data by removing that average from each occurrence of that month in the same record. The results using MA data are generally quite similar to those for data as supplied by CDC.

The monthly data used include SLP, and precipitation rate (hereafter: P) as supplied by CDC. The three remote forcing mechanisms all involve some type of divergent circulation where rising is presumed to occur at or near the site of the remote forcing. That rising motion is assumed to have associated precipitation. Hence, P data are used as a proxy for the remote forcing: higher P is presumed to be associated with a stronger remote forcing mechanism. However, P data are not an ideal proxy since precipitation is influenced by other factors than vertical motion. Further, the reanalysis P are determined by the reanalysis model instead of being directly assimilated. However, Kalnay et al. (1996) and Kistler et al. (2001) state that the reanalysis P data generally agree favorably with other published data. The use of the P data here seems reasonable in the context in which the data are used: emphasizing relative differences, seeking consistency with other variables, and using monthly means. A related variable is outgoing longwave radiation (OLR). The interpolated OLR data available from CDC (not a reanalysis product) are used. However, OLR has a latitudinal trend. Most of the calculations using P are duplicated using OLR; since the two give similar results only P data are displayed here.

For daily data, SLP, zonal wind, and meridional wind components were obtained

from CDC. From these, divergent wind components, and velocity potential were calculated. These data are emphasized in this study. The velocity potential is a smoother and likely more reliable field than daily P would be. However, velocity potential did not appear to be a useful indicator of divergent circulations associated with midlatitude frontal cyclones and so divergent wind components are used for that purpose. Data for contiguous December through February periods from 1979-2002 are used.

For the monthly data, the analysis tools are of two types: composites and "1-point" correlations. The composites consist of isolating the 6 instances of highest central pressure in the SP high, the 6 instances of lowest central pressure, and examining the difference between the two. (The sample size is small so the composites are formed from a small number of months. Tests using 8-month composites are essentially the same.) The statistical test is a simple (bootstrap) random resampling with replacement from the total sample (95 for the 1979-1997 period). The 1-point correlations use rank correlations (Press, et al., 1992) due to the nature of the data. (For example, precipitation data in some regions of interest are zero during several of the months.) We further require the data to pass both of two statistical significance tests upon the correlations relative to the population. One is an approximate "student's t" test and the other a test based on the sum of squared difference of ranks (see Press et al., 1992; p. 489-90). Plots often show a close correspondence between areas enclosed by the ≥0.3 correlation and areas passing both of the significance tests at the 1% level.

For the daily data the analyses are based upon 1-point correlations between the point values of SLP and another two-dimensional field at various lead and lag times. The two-dimensional fields emphasized here are velocity potential and divergent wind components. Lagged 1-point autocorrelations also prove useful. Lead and lag cross-correlations between a single SLP point and a single point of another variable illuminate a transition of events over time. Cross spectra are also calculated but the results are only able to identify a reliable signal in a limited range of low frequencies.

4. RESULTS FROM MONTHLY-MEAN DATA

Composites and "1-point" rank correlations of monthly-mean NCEP/NCAR reanalysis data were made to screen for evidence of the 3 remote forcing mechanisms. Monthly mean data cannot distinguish cause from effect since actual lags are likely shorter than a 1-month averaging period. Figure 2 shows the time mean SLP and P fields to assist with interpreting difference and correlation fields. Another purpose in presenting Figure 2 is to allow the reader to judge the 'reasonableness' of the P field.

Composites of conditions during unusually strong highs, weak highs, and strong minus weak highs were created with seasonal stratification and either total or MA data. MA data are shown in Figure 3 using a 19-year period. Work with OLR data obtains similar results as P data (not surprisingly). Figure 3 shows difference maps between the 6 strongest SP highs minus the 6 weakest SP highs drawn from all the October through February months during 1979-1997. By definition, the SLP difference is positive over the SP high. The SLP difference has associated lower SLP over most of South America. Small areas of lower SLP occur over and near Australia, which collectively may be important to note. While there is negative SLP difference to the South of the SP high it does not pass the significance test.

The corresponding difference pattern in P (Figure 3b) shows a dipolar pattern to the South of the SP high indicative of precipitation reduced on the south side of the SP high and enhanced further south; this pattern possibly indicates a southward shift of the frontal cyclone storm track (compare with Figure 2). Close comparison between Figures. 2b and 3b finds the following. P in the western equatorial Pacific is lessened where the time mean pattern has a transition between much higher P to the west and very little P to the east-southeast. P is enhanced along a diagonal line that is parallel to but southwest of the SPCZ axis. The time mean pattern of P has largest values along the SPCZ axis (Figure 2). The pattern clearly indicates that the SPCZ is shifted further away from the SP high when the high is stronger. To the north, P is enhanced along an east-west line centered both along and to the north of the ICZ. So, the mid-Pacific ICZ is strengthened

and partly shifted away (North) during stronger SP highs. Similar, though smoother patterns are obtained from the OLR data (not shown).

The 1-point correlations are broadly consistent with the composites results. Figure 4 shows correlations between the two dimensional P field and each SLP point from a group of points surrounding the SP high. Maps using OLR instead of P are similar (not shown). Also shown are correlations using the maximum SLP value. Shaded regions denote where two significance tests are both passed at the 1% or better level.

In general, Figure 4 shows that SLP on a given side of the SP high is associated with significant P changes on the corresponding side. Points to the northeast side (Figure 4b) associate exclusively to tropical P. Points on the east side (Figure 4d) have similar associations with P as points due north (not shown) and those associations are significant in higher and lower latitudes. On the northwest side (Figure 4a) of the SP high, SLP is linked to P over a wide range of latitudes, both higher and lower. For SLP points on the west (Figure 4c), southwest, south (Figure 4e) and southeast sides, there is little tropical P associated but a large dipole pattern in middle latitudes to the south and west. The peak value (Figure 4f) of the SP high is linked with more P over northern South America and a dipolar shift (southward) of P at higher latitudes. Longitudinal shifts (not shown) of the location of maximum SLP have a weak (dipole) association with corresponding shifts of the SPCZ and midlatitude storm track. These charts illustrate that the SP high is at an "interface" and linked to processes at higher latitudes and not just lower latitudes.

Higher SLP on the northeast and north sides are associated with enhanced P over Amazonia and a northward shift of the Pacific ICZ. Higher SLP on these sides, along with the east and northwest sides of the SP high are associated with less P in the western central Pacific (near Kiribati). SLP on the northwest side is linked to shifts of the Pacific ICZ (northward) and SPCZ (westward) away from the SP high. Higher SLP at points along the west, southwest, and south sides of the SP high is associated with a dipole pattern of P correlations that imply a poleward shift of the storm-track related P. MA data are shown in Figure 4; when "total" data (i.e., as supplied in CDC reanalysis fields) are

used the significance areas tend to be larger but otherwise are very similar. Only one notable difference was found: the MA and total data have opposite sign over eastern Amazonia for SLP points to the north and northeast of the SP high center. This suggests that total data can reveal the associations in most cases except for the indicated association. Peak values of the correlation exceed 0.5 in MA data in these places: over Amazonia, in the storm track southwest of the mean location of the peak value, and to the north of Papua New Guinea. (Total data have correlations exceeding 0.6.)

To the extent that P is a good proxy for each of the three remote forcing mechanisms, the monthly mean data show connections between the SP high and all three mechanisms. (When corresponding tests, not shown, are made for the NP high, two of the mechanisms are evident but the data are contradictory or at best weakly support the Rossby wavetrain mechanism. Further discussion of the NP high is beyond the scope of this report.) The monthly data show that all three mechanisms are linked on seasonal time scales. Two major issues remain. First, the time scale of the probable cause and effect is likely to be shorter than a month. Hence the results so far indicate associations, but not cause and effect. Second, since some of the links imply shifts of a P band away from the high when the high is stronger, an obvious question is whether the shift is a consequence rather than a cause of a stronger SP high. To address both types of issues, daily data are considered.

5. RESULTS FROM DAILY DATA

Time mean velocity potential (hereafter VP) at 200 hPa is shown in Figure 5. This mean pattern is constructed from daily data during all the contiguous December, January, and February months during 1979-2002. Since the region differs from that shown for the monthly mean data, the corresponding mean pattern of SLP is shown as well.

Before considering remote forcing mechanisms, it is instructive to note how the SLP field varies in a coordinated way. Autocorrelations between SLP at points on the north side of the SP high differ markedly from points on the South side. For points on the

north side, a large region of the tropics, extending well into the Northern Hemisphere, has significant positive correlation and the correlation varies slowly over time. Figure 6 shows these correlations at differing lead and lag times. Intriguingly, a negative correlation develops after several days and strengthens (to more than –0.5) over the region of Southeast Asia and Borneo reaching a peak at about 20 days lead. This area of negative correlation appears a similar period of time before zero lag, then diminishes as zero lag is approached. An obvious explanation is the Madden-Julian Oscillation (MJO) and the association with the MJO is explored later. An intriguing aspect is that the negative correlation over Borneo is greater when it peaks ~20 days *after* the higher SLP on the North side of the SP high, than when it peaks before.

For points to the south of the SP high the autocorrelation (not shown) is quite different. These autocorrelations are significant only over a small, disk-shaped region about 1000 km in radius or less. The disk shrinks rapidly as lag or lead increases; the radius is about half as large at 4 days lag (or lead) as it is at zero lag. The disk also moves from west to east similar to how midlatitude weather systems move.

Figure 7 shows the one-point correlation maps between SLP at a point on the equatorial side of the SP high and the two-dimensional velocity potential (VP) field at 200 hPa. Similar to the prior figure, correlations at different lead and lag times are shown. There is a run up of higher than normal SLP prior to the peak SLP, and during that time, there are already coincident changes in the velocity potential, hence the correlations are spread over lag and lead times. For that reason, cause and effect are a little hard to deduce since the changes are slow to evolve. Where the changes are more weighted to one side (lag or lead) will be our marker to distinguish cause or effect. Figures 7a-c show an area of negative correlation over Amazonia. This region already has negative values of VP and associated strong convective activity. So, higher SLP at this point on the north side of the SP high is associated with enhanced convection over Amazonia. Figure 7 also shows a large area of positive correlation over the western equatorial and southwestern Pacific, an area of mainly negative values of VP. This pattern indicates stronger SLP on the north side of the SP high is linked to weakened convection where it is normally strong. This

large area of positive correlation is moving towards the east and persisting after the peak SLP is reached, suggesting that the stronger SLP leads the suppression of the convection, but that pattern itself is moving eastward. At later times (Figures 7d-e) positive correlation moves over regions where VP is positive (the East Pacific, recall Figure 5) so the maximum in VP in the East Pacific is enhanced, suggesting that the stronger SP high is reinforcing upper level convergence equatorward of the SP high at times after the peak SLP occurs. Finally, negative correlations develop over Southeast Asia and Borneo region at later times (contrasting Figures 7e and 7a). From Figure 5, this implies even stronger negative VP in that region which is consistent with lowering of SLP noted in the autocorrelation charts (Figure 6).

Figure 8 shows cross correlations between an SLP point on the northeast side of the SP high and various points in the VP field, as indicated on the chart. VP at Amazonian points (Figures 8g and 8h) has negative cross-correlations that peak 2 to 4 days in advance of the higher SLP. The cross correlation rapidly dips to zero after the peak occurs in SLP, so that enhanced Amazonian convection clearly precedes the SLP change. This relationship seems consistent with the Rossby wavetrain point of view in that the Amazonian convection is equatorward and east of the location at which SLP is tested. However, one might also argue that this result is consistent with the tropical divergent circulations view in the sense that the divergent circulation in the region extending from Amazonia to include the northeastern side of the SP high itself is clearly directed from the former to the latter at upper levels. (One may deduce that circulation as parallel to and up the gradient of VP in Figure 8k.) Whether this reveals a connection between the two mechanisms or a coincidence is beyond the intent of this report.

Figure 8 also shows coordinated changes in the western Pacific VP prior to the higher SLP on the northeast side of the SP high. The positive cross-correlation (implying weakening of the strong negative values) occurs at progressively earlier times as the VP correlation point is moved west. Over Papua New Guinea (Figure 8a), the peak correlation occurs 3 days prior, near the dateline (Figures 8b then 8c) the peak is 2 days prior and further east (Figure 8d) the peak is only 1 day prior. In addition, the cross

correlations over Australia, New Guinea, and the equatorial Pacific have a monotonic trend for the next 3 weeks before reaching a peak negative correlation and reversing the trend. The cross-correlation pattern over these regions thus has a strong period on the order of 45 days in cross spectra (not shown). The MJO has a similar period and one expects a connection since it is well known that tropical Pacific convection is modulated by the MJO. The next section shows a strong correlation between MJO and SLP on the tropical side of the SP high. To the south of the SP high, positive correlations (Figures 8i and 8j) lag behind the peak values at the SLP correlation point on northeast side of the SP high, perhaps indicating a response to the change on the northeast side.

Figures 7 and 8 indicate that stronger SLP values on the equatorial side of the SP high occur when the convection over Amazonia and Indonesia are coordinated as follows. Expansion of the Amazonian VP minimum (enhanced convection, especially over northern South America) plus weaker minimum VP (reduced convection) over Indonesia, New Guinea, and Australia lead to higher SLP on the northeast side of the SP high. A similar (though weaker) trend is evident in cross-correlations for SLP points on the North side of the SP high (not shown).

Figure 8 also shows cross-correlations for a VP point (Figure 8f) near the SLP correlation point and a VP point (Figure 8e) near the maximum in VP. At both points VP>0. Both points show negative cross-correlation prior to the SLP high maximum, roughly zero correlation at the time of SLP maximum, and positive correlation afterwards. The pattern is noted in Figure 7 and reveals expansion of the Amazonian VP minimum followed by expansion of the East Pacific VP maximum. Note that the highest SLP does not occur at the same time as a significant VP cross-correlation at this spot. This may be surprising if one expects higher SLP to be linked to stronger sinking at the same spot.

Figure 9 is similar to Figure 7 except illustrating higher latitude associations. The two dimensional field is the meridional component of divergent wind (Vd) at 200 hPa. The SLP point is poleward of the time mean position of the SLP maximum. Darker

(lighter) shaded areas containing solid (dashed) contour lines in figures 9b-f indicate northward (southward) anomalous motion that is statistically significant when the SLP at the correlation point is higher than normal. The lags and lead times shown are more closely spaced than in Figure 7 because events happen more quickly on this side of the SP high and because the correlations diminish more rapidly as the lag or lead time increases. The areas of significant correlation move from west to east, as do transient midlatitude cyclones and anticyclones. The pattern of shading is dipolar: a significant area of upper level southward anomalous divergent wind is just north of a significant area of northward anomalous divergent wind on most plots (Figures 9c-e). The zonal component of divergent wind (not shown) does not show any significant dipole pattern that could provide compensating divergence, so the dipole pattern in Figure 9 suggests enhanced upper level convergence to the east of the SP high a day or so before the SLP beneath is made larger. (In Figure 9, the strongest cross-correlation is at day 0, but located to the east of the SLP correlation point.)

Stronger SP high central pressure occurs when the location of the peak value is southwest of the mean position. When the peak value is tracked (and not a fixed point) the cross-correlations at various lags and leads look similar to the sequence of plots in Figure 9. Figure 10 reinforces the connection between SP high central pressure and higher latitude events. Figure 10 is similar to Figure 8 except using the divergent wind speed (DWS) and maximum SLP value. DWS is plotted in Figure 10k. Consistent with Figure 9, the cross-correlations are generally small, particularly for the tropical DWS points. The cross-correlations in Figures 10a-10g are shown to demonstrate the small size of these correlations. Figure 10d is illustrative of other points (not shown) astride and along the Pacific ICZ. Figure 10f is intended to test for Atlantic ICZ association. At higher latitudes than the SP high (Figures 10h-10j) the cross correlations have narrow peaks (consistent with the short periods of significant correlation). Only DWS points to the south of the SP high have cross-correlations exceeding 0.2. Comparing Figures 10h, 10i, and 10j, the peak cross-correlation (positive) occurs at progressively earlier times the further away the DWS point is from the SP high. This progression is consistent with an eastward and northward propagating signal. These data suggest that the SP high

maximum is not preceded by tropical events in any strong way. These data are consistent with the midlatitude forcing mechanism. Further identification of the precise phenomena or nature of the mechanism(s) is beyond the scope of this study.

6. ASSOCIATIONS WITH STANDARD INDICES

Since strong connections have been shown between the SP high and tropical Pacific precipitation, an obvious extension of the work is to consider meteorological and oceanic indices that relate to tropical Pacific precipitation, namely those associated with "El Nino – Southern Oscillation" (ENSO) and those associated with the Madden-Julian Oscillation (MJO). A summary of ENSO properties can be found in Philander (1990). A summary reference for the MJO is Madden and Julian (1994).

A primary measure of ENSO activity is the Southern Oscillation Index (SOI) constructed from monthly mean standardized SLP anomalies for Tahiti and Darwin. An alternative measure of ENSO is the sea surface temperature (SST) anomaly in the central-eastern equatorial Pacific. A key SST is the anomaly from two regions combined and given the name "Nino 3+4". Correlations between SOI and Nino 3+4 and monthly SLP are shown in Figure 11. Since Nino 3+4 tends to be positive when the SOI is negative, their correlations with SLP will tend to have opposite sign. SOI is derived from SLP at Tahiti, so the highest positive correlation in Figure 11b occurs there. For both indices the SLP on the equatorial side of the SP high has significant correlation > 0.3. The correlation drops rapidly on the higher latitude side of the SP high. This result is broadly consistent with associations shown above to the extent that these indices identify longitudinal shifts of the strongest equatorial precipitation. A slight inconsistency is that areas of significant correlation in figure 11 just reach the latitude of the climatological SP high center whereas SLP at the latitude of the SP high center is not significantly correlated to other proxies of tropical convection shown earlier.

The MJO is a principal mode of time variation of tropical convection, particularly in the western tropical Pacific. Since SLP on the tropical side of the SP high is associated

above with suppression of western tropical Pacific convection, one expects a similar connection between the SP high and the MJO. The MJO has long been known (Madden and Julian, 1971; 1972) to have a signature in tropical SLP. The questions are how far into the subtropical South Pacific latitudes does the association between MJO and SLP extend and which comes first. To address these questions, a measure of MJO activity is cross correlated with SLP data across the South Pacific. Seasonally independent indices developed by Wheeler and Hendon (2004; see website: http://www.bom.gov.au/bmrc/clfor/cfstaff/matw/maproom/RMM/) are used. Wheeler and Hendon's indices are based upon time series of the first two principal components obtained from a combined analysis of OLR, and 200 and 850 hPa zonal wind along the equatorial zone. Cross correlations (not shown) using Wheeler and Hendon's two indices find no significant associations except for the SLP points in the equatorial side of the SP high. Of the points shown in figure 4, cross correlations at points used in figures 4a and 4b have ensemble average correlations with peak values near -/+0.4. Higher SLP at the "NE" point in figure 4b is preceded by peak positive OLR over the Indian Ocean (11-12 days before at 80E) then over Indonesia (2-3 days before at 120-150E) and followed by peak positive OLR near the dateline (4 days later at 150-200E). These results are broadly consistent with the VP data shown in figure 8. The results are also consistent with Kayano and Kousky (1999; their figure 4) who use an MJO-like extended empirical orthogonal function, EEOF, to define an intraseasonal index. Their EEOF is based on 200 hPa velocity potential. Kayano and Kousky find correlations exceeding 0.3 only on the equatorial side and wrapping around the east edge into the latitude of the SP high center.

Climate indices such as the MJO and SOI raise the prospect of teleconnections between anomalous tropical convection and midlatitude circulations. Numerous authors have investigated such connections (e.g. Hoskins and Karoly, 1981). In the Southern Hemisphere, a primary mode of variability identified in upper level flows is the "Pacific South American" (PSA) mode. For example, Kidson (1991) identifies this mode centered near 50S across the Pacific having approximate scale of zonal wavenumber 4. The mode occurs as a pair in quadrature and the implied propagation is found by Kidson to be about 4-7^{o} longitude per day at 55S. However, Kidson concludes that this mode does not

interact with lower latitudes. In contrast, other studies (e.g. Mo and Higgins, 1998; Renwick and Revell, 1999) attempt to trace this mode back to convection in the tropical west Pacific – Indonesia region. Mo and Higgins (using 200 hPa zonal-deviation stream function Ψ) note that the PSA has a shorter period than the intraseasonal oscillation in equatorial latitudes. Mo and Higgins (1998) further conclude that an oscillation like the MJO may not cause the PSA but when the tropical intraseasonal oscillation is "strong" then that may catalyze or foster the PSA to be stronger; thereby bridging the apparent gap with Kidson (1991). The PSA is usually implicated as a blocking pattern in the South Pacific and as such most studies focus on the upper troposphere. One should not equate an upper level block with the subtropical high. However, variability in the subtropical high may be created by waxing and waning blocking patterns. Also, even though it is commonly stated that blocks are "equivalent barotropic", one should not expect the SLP pattern to underlie 500 hPa geopotential height (Z) pattern. However, the PSA in Z does have a similar signature at low levels; with a small phase shift (~10^{o} longitude, or ~1/9 of a wavelength) westward from 1000 to 500 hPa (Kidson, 1991; his figure 5). The PSA in 1000 hPa Z has a weak signature in the central and tropical part of the SP high. In Mo and Higgin's figure 1, a weak secondary extreme in 200 hPa Ψ lies northwest of the SP high center. So, the PSA pattern largely skirts around the southern fringe of the SP high and possibly overlies to the tropical side. Since the PSA is the best known midlatitude connection to the MJO, the PSA pattern may explain why the SP high has little association to the MJO except on the equatorial fringe of the SP high.

7. SUMMARY

This study finds observational evidence that appears to support three proposed remote forcing mechanisms of the South Pacific subtropical high (SP high). Various observed fields are used as proxy indicators of the divergent circulation that is presumed to be associated with each remote mechanism. Tropical sources of forcing tend to affect just the equatorward side of the SP high. Higher latitude forcing tends to affect the poleward side and western side of the SP high. These results are consistent with the

notion that a subtropical high results from the interplay of forcing from higher as well as lower latitudes.

In monthly data, one-point correlations find stronger SLP on the north and west sides of the SP high when the ICZ and SPCZ respectively, are shifted away from the high. These shifts cause reduced precipitation in the western equatorial Pacific. Since ENSO is a strong signal in monthly data of the tropical western Pacific, correlations with ENSO are significant with SLP changes, but only on the north and east sides of the SP high. Stronger high composites are also cases with lower SLP over most of South America and the Drake Passage. However, stronger precipitation is not seen over South America in the monthly mean composites, though higher precipitation is seen over the adjacent tropical Atlantic. The strongest change in P seen in monthly composites is a shift of the extreme southern end of the SPCZ to the south for stronger SP highs. Daily data illuminate how these associations proceed.

Daily data show SLP on the equatorial and northeast sides of the SP high to be highly autocorrelated with SLP in the equatorial and East Pacific, even into the subtropics of the Northern Hemisphere. Stronger SLP on the north side of the SP high is followed by lower SLP over Southeast Asia peaking 3 weeks later. Stronger SLP on the north and northeast sides is favored several days after weaker convection occurs near Papua New Guinea (deduced from weakened negative velocity potential, VP) along with expansion of the Amazonian VP minimum (especially on its North side). Stronger SLP at those sides is followed in a few days by a westward shift of the eastern Pacific VP maximum. This last item leads a westward migration of higher than normal SLP on the equatorial side of the SP high. For many points, the cross spectrum has a strong frequency peak around 45 days. The spectral frequency peak and its western equatorial Pacific prominence indicate an MJO-like signal. Indeed, stronger SLP on the equatorial and northeast sides of the SP high are well correlated (0.4) with the phase of the MJO indicating convection suppressed over Indonesia.

Stronger SP highs tend to occur when the location of maximum SLP is southwest of the mean position in monthly and daily data. In daily data stronger highs occur when reinforced by upper level convergence just to the south and east. This convergence would foster sinking and presumably strengthen surface southerlies as emphasized by Shaffrey et al. (2002) except that the strengthened convergence arises from midlatitude, not tropical divergent winds. The lack of tropical correlation, the rapid rate of eastward progression, and the midlatitude prominence of the area of upper level convergence suggest the associated divergent winds are driven by midlatitude weather systems. The maximum in SP high has little or no significant correlation to tropical weather in daily data. At first glance this result seems to contradict the monthly data composites, wherein stronger SP highs also have associated lower SLP over Amazonia and the tropical Atlantic. Furthermore, the strong high composite has associated enhanced P over the tropical Atlantic. The data suggest that a connection to Amazonia occurs in composites because the composites of stronger SP highs have enhanced SLP over a broad area that includes the east and tropical sides of the SP high, not just the maximum SLP value.

ACKNOWLEDGEMENTS

The NCEP/NCAR Reanalysis data used in this study were provided by the NOAA-CIRES Climate Diagnostics Center, Boulder, Colorado, USA, from their Web site at http://www.cdc.noaa.gov/. The author appreciates many discussions with participants at the three conferences listed. Assistance by Dr. G. Kiladis is particularly appreciated. I thank K. Weickmann for assistance finding an MJO dataset and M. Wheeler for providing daily MJO indices. Two anonymous reviews were very helpful as well. Some of the calculations were performed using computers at the National Center for Atmospheric Research, Climate and Global Dynamics Division, whose support is greatly appreciated.

REFERENCES

Blackmon, M., Wallace, J., Lau, N.-C., Mullen, S., 1977. An observational study of the Northern Hemisphere wintertime circulation. *Journal of the Atmospheric Sciences*, **34**: 1040-1053.

Carlson T., 1994. *Mid-Latitude Weather Systems*. Routledge, London, 507 pp.

Chen P., Hoerling M., Dole R., 2001. On the origin of the subtropical anticyclones. *Journal of the Atmospheric Sciences*, **58**: 1827-1835.

Gill A., 1980. Some simple solutions for heat-induced tropical circulation. *Quarterly Journal of the Royal Meteorological Society*, **106**: 447-462.

Grotjahn R., 1993. *Global Atmospheric Circulations: Observations and Theories*. Oxford, 430pp.

Grotjahn R., 2000. Causes of seasonal change in the South Pacific subtropical high (oral), 6th Int'l Conf. on Southern Hemisphere Meteorology and Oceanography, Santiago Chile, AMS, 352-353.

Grotjahn R., Immel S., 2001. Observational study of the remote forcing of the Pacific subtropical highs (poster), 13th Conf. on Atmospheric and Oceanic Fluid Dynamics, Breckenridge USA, AMS, 16-17.

Grotjahn R., 2003. Remote features linked to the South Pacific subtropical high (oral), 7th Int'l Conf. on Southern Hemisphere Meteorology and Oceanography, Wellington NZ, AMS, 1-2.

Heckley W., Gill A., 1984. Some simple analytical solutions to the problem of forced equatorial long waves. *Quarterly Journal of the Royal Meteorological Society*, **110**: 203-217.

Holton J., 1992. *An Introduction to Dynamic Meteorology*, 3rd ed., Academic, San Diego, 511pp.

Hoskins B., 1996. On the existence and strength of the summer subtropical anticyclones. *Bulletin of the American Meteorological Society*, **77**: 1287-1292.

Hoskins, B., Karoly, D., 1981. Steady linear response of a spherical atmosphere to thermal and orographic forcing. *Journal of the Atmospheric Sciences*, **38**: 1179-1196.

Hoskins B, Neale R., Rodwell M., Yang G.-Y., 1999. Aspects of the large-scale tropical atmospheric circulation. *Tellus*, **51A-B**: 33-44.

Hoskins B., Rodwell M., 1995. A model of the Asian summer monsoon. Part I: The global scale. *Journal of the Atmospheric Sciences*, **52**: 1329-1340.

Jones, D., Simmonds, I., 1994. A climatology of Southern Hemisphere anticyclones. Climate Dynamics, **10**, 333-348.

Kalnay E., Kanamitsu M., Kistler R., Collins W., Deaven D., Gandin L., Iredell M., Saha S., White G., Woollen J., Zhu Y., Leetmaa A., Reynolds R., Chelliah M., Ebisuzaki W., Higgins W., Janowiak J., Mo K., Ropelewski C., Wang J., Jenne R., Joseph D., 1996. The NCEP/NCAR 40-year reanalysis project. *Bulletin of the American Meteorological Society*, **77**: 437-471.

Kayano, M., Kousky, V., 1999. Intraseasonal (30-60 day) variability in the global tropics: principal modes and their evolution. *Tellus*, **51A**: 373-386.

Kidson, J., 1991. Intraseasonal variations in the Southern Hemisphere circulation. *Journal of Climate*, **4**: 939-953.

Kistler R., Kalnay, E., Collins, W., Saha, S., White, G., Woollen, J., Chelliah M., Ebisuzaki, W., Kanamitsu, M., Kousky, V., van den Dool, H., Jenne, R., Fiorino, M., 2001. The NCEP/NCAR 50-year reanalysis, *Bulletin of the American Meteorological Society*, **82**: 247-267.

Leighton, R., 1994. Monthly anticyclonicity and cyclonicity in the Southern Hemisphere: Averages for January, April, July and October. *International Journal of Climatology,* **14**, 33-45.

Madden, R., Julian, P., 1971. Detection of a 40-50 day oscillation in the zonal wind in the tropical Pacific. *Journal of the Atmospheric Sciences*, **28**: 702-708.

Madden, R., Julian, P., 1972. Description of global-scale circulation cells in the tropics with a 40-50 day period. *Journal of the Atmospheric Sciences*, **29**: 1109-1123.

Madden, R., Julian, P., 1994. Observations of the 40-50-day tropical oscillation – a review. *Monthly Weather Review*, **122**, 814-837.

Mo, K., Higgins, R., 1998. The Pacific-South American modes and tropical convection during the Southern Hemisphere winter. *Monthly Weather Review*, **126**: 1581-1596.

Oort A., Peixoto J., 1983. Global angular momentum and energy balance requirements from observations. *Advances in Geophysics*, **25**: 355-490.

Pfeffer R., 1981. Wave-mean flow interactions in the atmosphere. *Journal of the Atmospheric Sciences*, **38**: 1340-1359.

Philander, G., 1990. *El Nino, La Nina, and the Southern Oscillation*. Academic, San Diego, 293 pp.

Press W., Flannery B., Teukolsky S., Vetterling W., 1992. *Numerical Recipes, The Art of Scientific Computing*. Cambridge, NY, 702 pp.

Renwick, J., Revell, M., 1999. Blocking over the South Pacific and Rossby wave propagation. *Monthly Weather Review*, **127**: 2233-2247.

Shaffrey L., Hoskins B., Lu R., 2002. The relationship between the North American summer monsoon, the Rocky Mountains and the North Pacific subtropical anticyclone in HadAM3. *Quarterly Journal of the Royal Meteorological Society*, **128**: 2607-2622.

Sinclair, M., 1996. A climatology of anticyclones and blocking for the Southern Hemisphere. *Monthly Weather Review*, **124**: 245-263.

Taljaard, J., 1967. Development, distribution and movement of cyclones and anticyclones in the Southern Hemisphere during the IGY. *Journal of Applied Meteorology*, **6**, 973-987.

Trenberth K., Shea D., 1987. On the evolution of the southern oscillation. *Monthly Weather Review*, **115**: 3078-3096.

Wallace J.M., 1983. The climatological mean stationary waves: observational evidence In: *Large-Scale Dynamical Processes in the Atmosphere*. Hoskins B., Pearce R., eds. Academic Press, London, 27-53

Wheeler, M., Hendon, H., 2004. An all-season real-time multivariate MJO index: Development of an index for monitoring and prediction. *Monthly Weather Review. In press.*

FIGURE CAPTIONS

Figure 1. Monthly mean maximum sea level pressure (SLP) for the South Pacific (SP) and North Pacific (NP) subtropical highs. Darker line with diamonds is the median while the dot-dashed line with "x" marks is the mean. Lines with triangles and squares are the first and third quartiles in the 24-year period from 1979-2002. The SP high is strongest during spring while the NP high is strongest during mid summer.

Figure 2. Time means of a) SLP and b) precipitation (P) constructed from November-February months during 1979-1997. The darkest band in each panel is for the ranges 996-998 hPa SLP and 7-9 mm/day P. In a) the light shaded region greater than 1018 hPa is the SP high. In b), the South Pacific convergence zone (SPCZ) is the diagonal band of higher P from the equatorial West Pacific towards the Southeast Pacific. The intertropical convergence zone (ICZ) is the east-west oriented band of higher P across the equatorial Pacific and a similar band in the equatorial Atlantic. The South American convergence zone (SACZ) is a diagonal band of higher P across South America. The contour intervals are 4 hPa and 1 mm/day.

Figure 3. Composite difference maps between the 6 months of strongest SP highs minus the 6 months of weakest SP highs selected from the October-February months during 1979-1997. Shaded areas having a dark border are significantly lower values; shaded areas without a dark border are significantly higher values. a) SLP; b) P. By definition, the SLP difference is positive over the SP high. Stronger SP high composite has dipole in P to the Southwest of the high and more precipitation along the sides of the ICZ and SPCZ further from the SP high. The contour intervals are 2 hPa and 1 mm/day; dashed contours indicate negative values. See text for discussion.

Figure 4. 1-point rank correlation maps for the two dimensional field of P against SLP at the point indicated by the circled X. H marks the location of the time mean SP high center. The direction of the circled X from the H location is indicated in the lower left

corner of each map. a) NW of H; b) NE of H; c) W of H; d) E of H; e) S of H; f) maximum value of SLP. Correlations are contoured starting at 0.3 and using a 0.1 interval. Shading encloses areas passing a pair of significance tests at the 1% or better level. Areas with lighter shading also have dashed contour lines and are negative correlations. Darker shaded regions are positive correlations and have solid contour lines. Monthly anomaly data are used. See text for discussion.

Figure 5. Time mean of: a) daily SLP and b) velocity potential (VP) using all contiguous December, January, and February months from 1979-2002. SLP contour interval is 2.5 hPa. VP contour interval is 10^6 m^2 s^{-1}.

Figure 6. SLP autocorrelations at various lags and lead times for a point (indicated by the circled asterisk) on the north side of the SP high. H marks the location of the time mean SP high center. Correlation contours start at 0.3 with a 0.1 interval. Negative correlations passing both of 2 significance tests at the 1% level have lighter shading with dashed contours; whereas positive correlations are denoted with darker shading and solid contours. In a) the correlation point values lag the two-dimensional field values by 12 days. The timing of the correlations shown is as follows: a) 12 days lag, b) 4 days lag, c) zero lag, d) 4 days lead, e) 12 days lead. Hence, the time evolution of the two dimensional field relative to the correlation point progresses clockwise on these diagrams, starting with a) and ending with e).

Figure 7. Similar to Figure 6 except for 1-point correlations between SLP at a point and the two dimensional field of VP. The SLP correlation point is on the North side of the SP high and marked by a circled asterisk. H marks the location of the time mean SP high center. Analogous to Figure 6, the time of the VP field progresses clockwise, occurring 8 days before the SLP at the correlation point in a) and proceeding to 8 days after the SLP value in e). Areas of negative significant (at 1% level) correlation have light shading and dashed contours. Darker shading and solid contours denote areas of positive significant correlation. The lowest contour magnitude is 0.3 and a 0.1 interval is used. The times shown are a) 8 days lag, b) 4 days lag, c) zero lag, d) 4 days lead, e) 8 days lead.

Figure 8. a) – j) Cross-correlation functions between SLP at point "P" and various locations marked on k) the contour plot of VP. "M" marks the location of the maximum in SLP. Point P is on the northeast side of the SP high. VP contour interval is 10^6 m^2 s^{-1}. The cross-correlation diagrams also indicate the timing of the VP maximum or minimum relative to the SLP data. In a) the maximum cross-correlation at the point in Papua New Guinea occurs when the VP data used is 3 days before the corresponding SLP data at point P. See text for discussion.

Figure 9. a) Time mean meridional component of divergent wind (Vd) at 200 hPa for all contiguous December, January, and February months during 1979-2002. Northward motion (Vd>0) is contoured using solid lines. Southward motion (Vd<0) is contoured with dashed lines. The contour interval is 0.5 m/s. To better distinguish northward from southward areas, areas of northward motion between 0-2.5 m/s have light or dark shading. b) – f) are similar to Figure 7 except using Vd and a SLP correlation point (indicated by the circled asterisk) on the south side of SP high. Timing of the Vd field relative to the SLP correlation point progresses clockwise from b) to f). In b) the values of Vd are correlated with SLP values 4 days later at the correlation point. The time mean position of the SP high is marked by H. Times shown are b) 4 days lag, c) 2 days lag, d) zero lag, e) 2 days lead, and f) 4 days lead. The south side of the SP high is enhanced by upper level convergence from traveling midlatitude cyclones.

Figure 10. a) – j) Cross-correlation functions between the SLP maximum value and various locations marked on k) the contour plot of divergent wind speed (DWS) at 200 hPa. The DWS contour interval is 1 m/s. The cross-correlation diagrams also indicate the timing of the VP maximum or minimum relative to the SLP data. In i) the maximum cross-correlation at the point in the central South Pacific occurs when the DWS data used are 2 days before the corresponding SLP data. a) – g) do not have cross-correlations exceeding 0.2 in magnitude so no maximum or minimum times are identified. See text for discussion.

Figure 11: a) Correlation between SLP and an equatorial central Pacific sea surface temperature anomaly index (Nino 3+4). b) Correlation between SLP and the Southern Oscillation Index (SOI). Contours start with magnitude 0.3 and change with 0.1 interval; dashed contours used for negative correlations. Areas of negative correlation passing a pair of 1% significance tests are shaded lightly; darker shading is used for positive significant correlations.

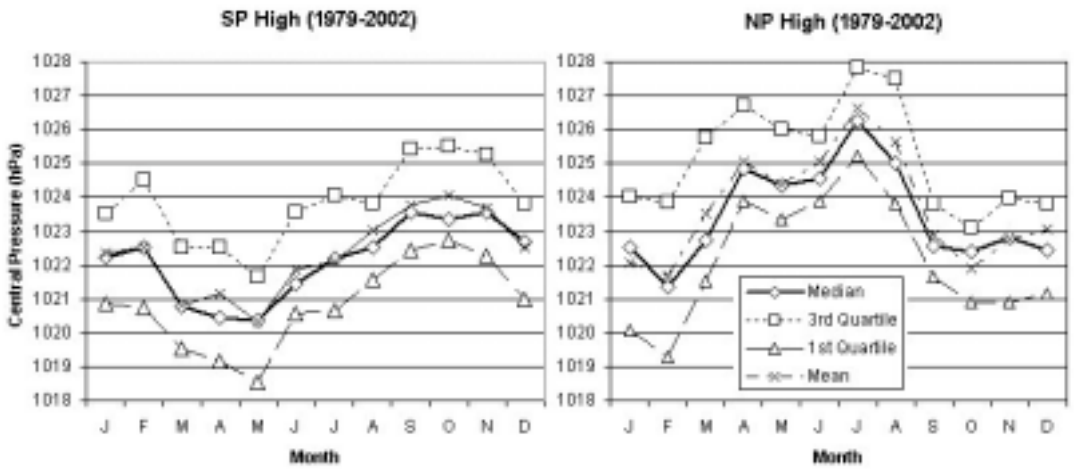

Figure 1. Monthly mean maximum sea level pressure (SLP) for the South Pacific (SP) and North Pacific (NP) subtropical highs. Darker line with diamonds is the median while the dot-dashed line with "x" marks is the mean. Lines with triangles and squares are the first and third quartiles in the 24-year period from 1979-2002. The SP high is strongest during spring while the NP high is strongest during mid summer.

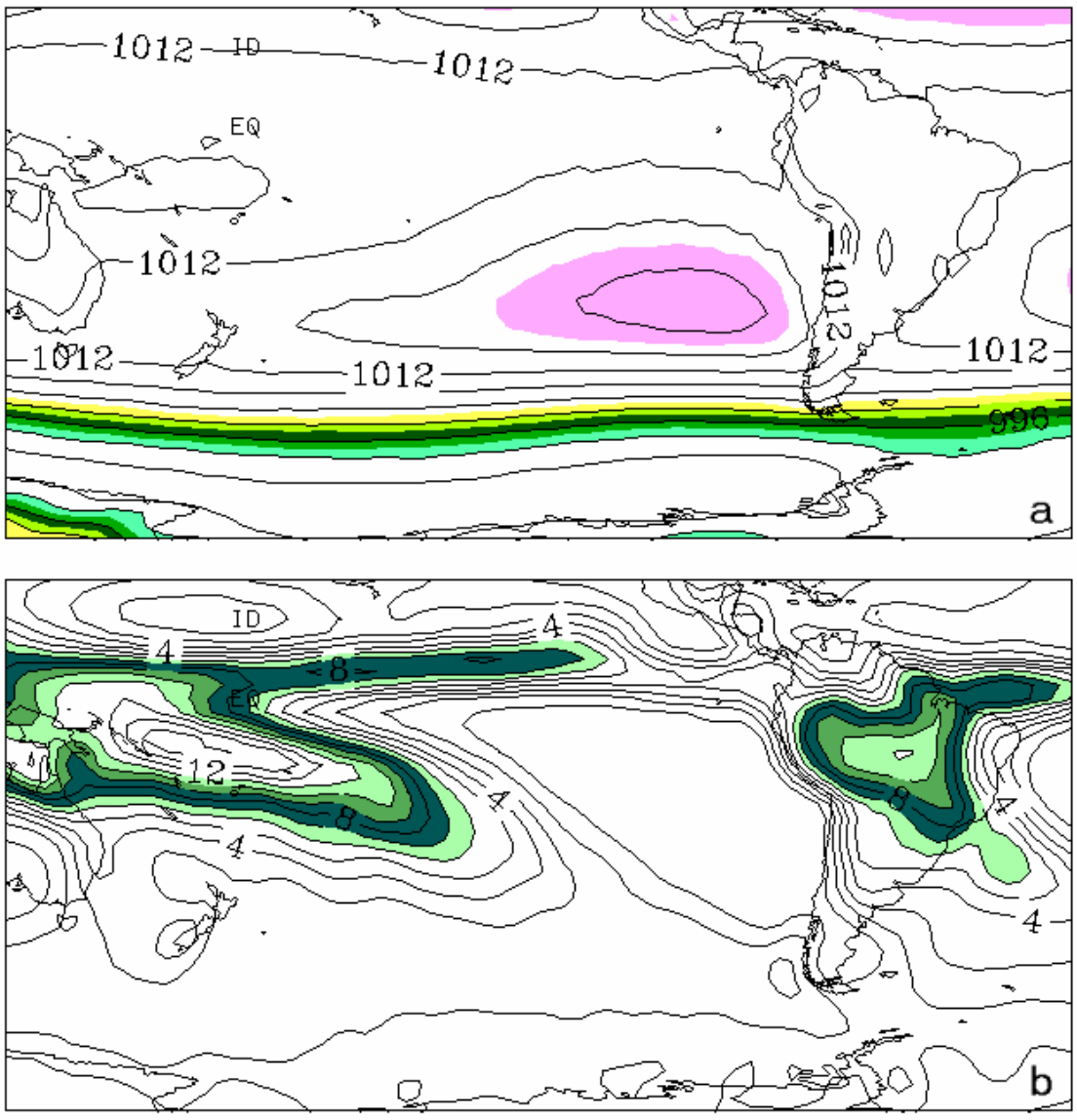

Figure 2. Time means of a) SLP and b) precipitation (P) constructed from November-February months during 1979-1997. The darkest band in each panel is for the ranges 996-998 hPa SLP and 7-9 mm/day P. In a) the light shaded region greater than 1018 hPa is the SP high. In b), the South Pacific convergence zone (SPCZ) is the diagonal band of higher P from the equatorial West Pacific towards the Southeast Pacific. The intertropical convergence zone (ICZ) is the east-west oriented band of higher P across the equatorial Pacific and a similar band in the equatorial Atlantic. The South American convergence zone (SACZ) is a diagonal band of higher P across South America. The contour intervals are 4 hPa and 1 mm/day.

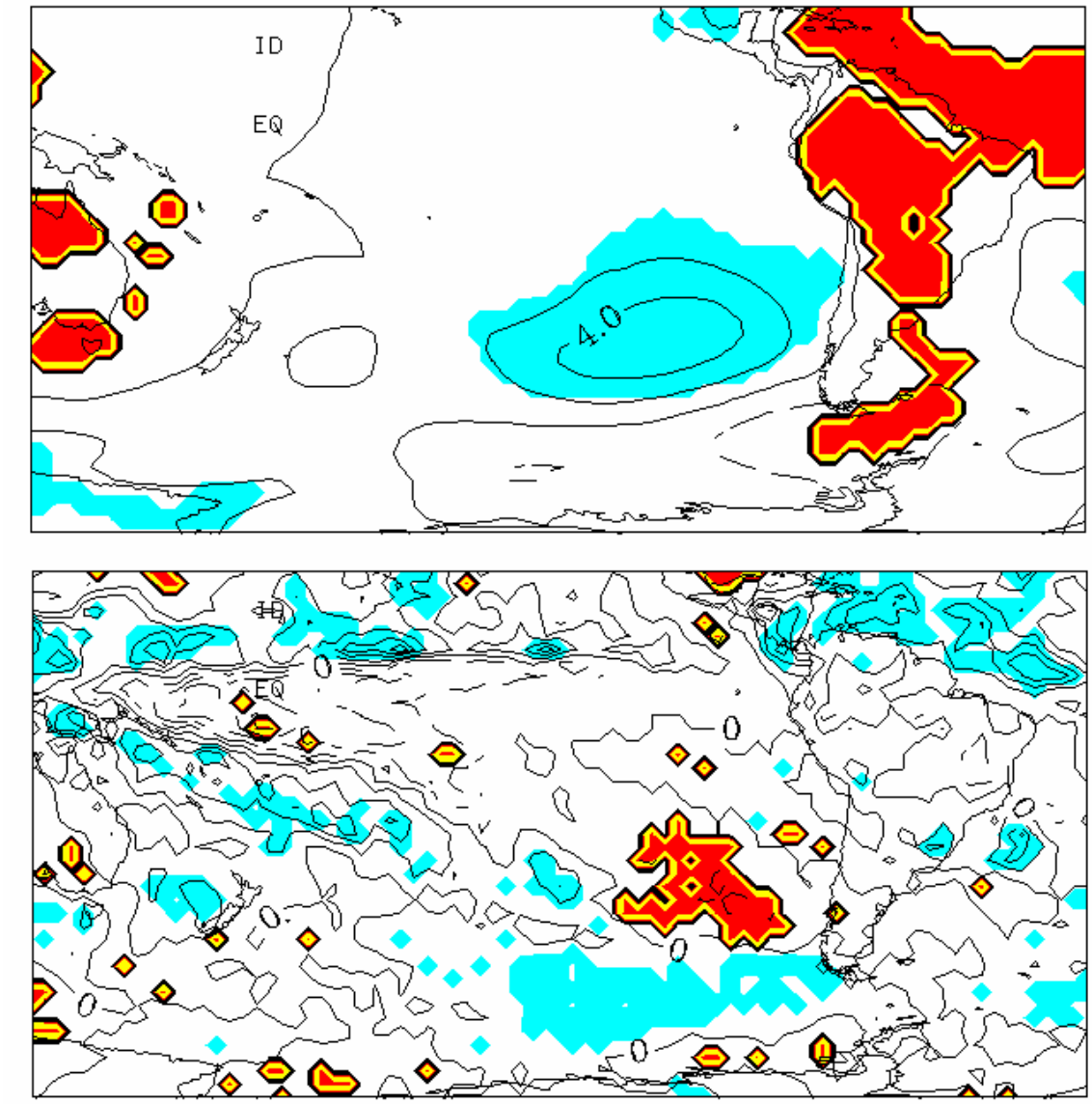

Figure 3. Composite difference maps between the 6 months of strongest SP highs minus the 6 months of weakest SP highs selected from the October-February months during 1979-1997. Shaded areas having a dark border are significantly lower values; shaded areas without a dark border are significantly higher values. a) SLP; b) P. By definition, the SLP difference is positive over the SP high. Stronger SP high composite has dipole in P to the Southwest of the high and more precipitation along the sides of the ICZ and SPCZ further from the SP high. The contour intervals are 2 hPa and 1 mm/day and dashed contours indicate negative values. See text for discussion.

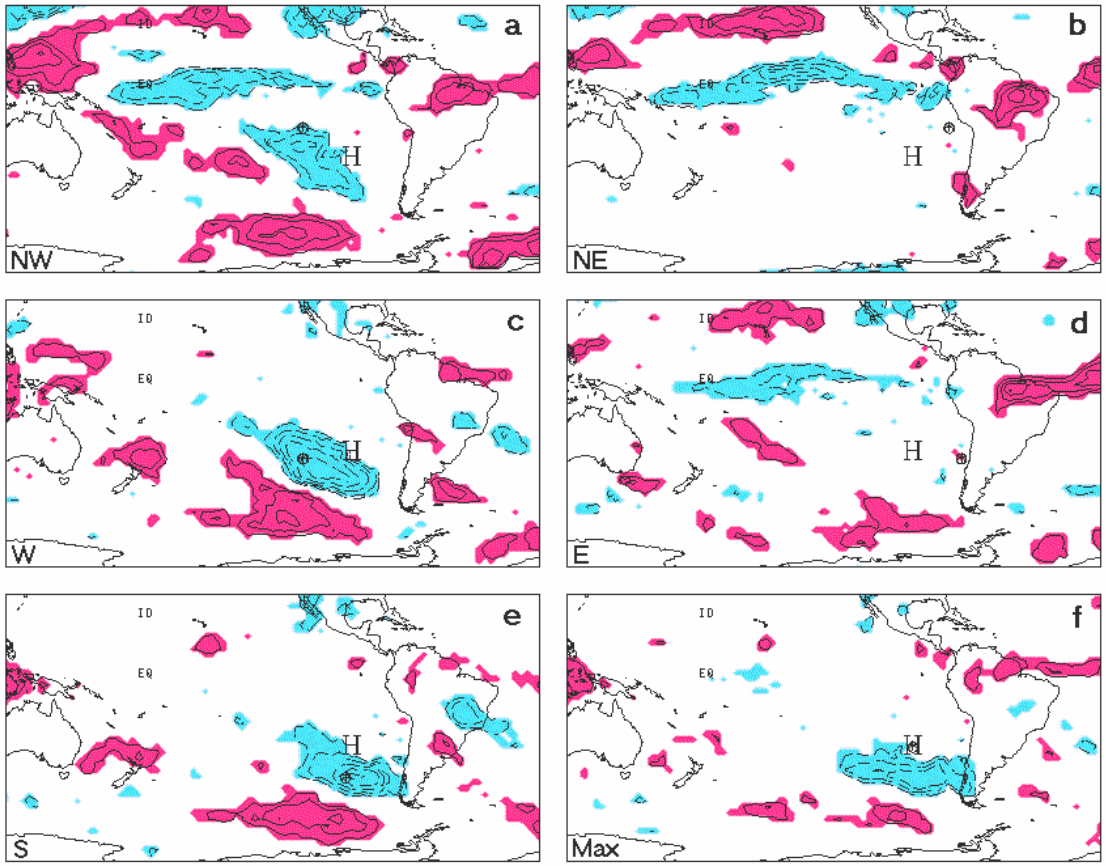

Figure 4. 1-point rank correlation maps for the two dimensional field of P against SLP at the point indicated by the circled X. H marks the location of the time mean SP high center. The direction of the circled X from the H location is indicated in the lower left corner of each map. a) NW of H; b) NE of H; c) W of H; d) E of H; e) S of H; f) maximum value of SLP. Correlations are contoured starting at 0.3 and using a 0.1 interval. Shading encloses areas passing a pair of significance tests at the 1% or better level. Areas with lighter shading also have dashed contour lines and are negative correlations. Darker shaded regions are positive correlations and have solid contour lines. Monthly anomaly data are used. See text for discussion.

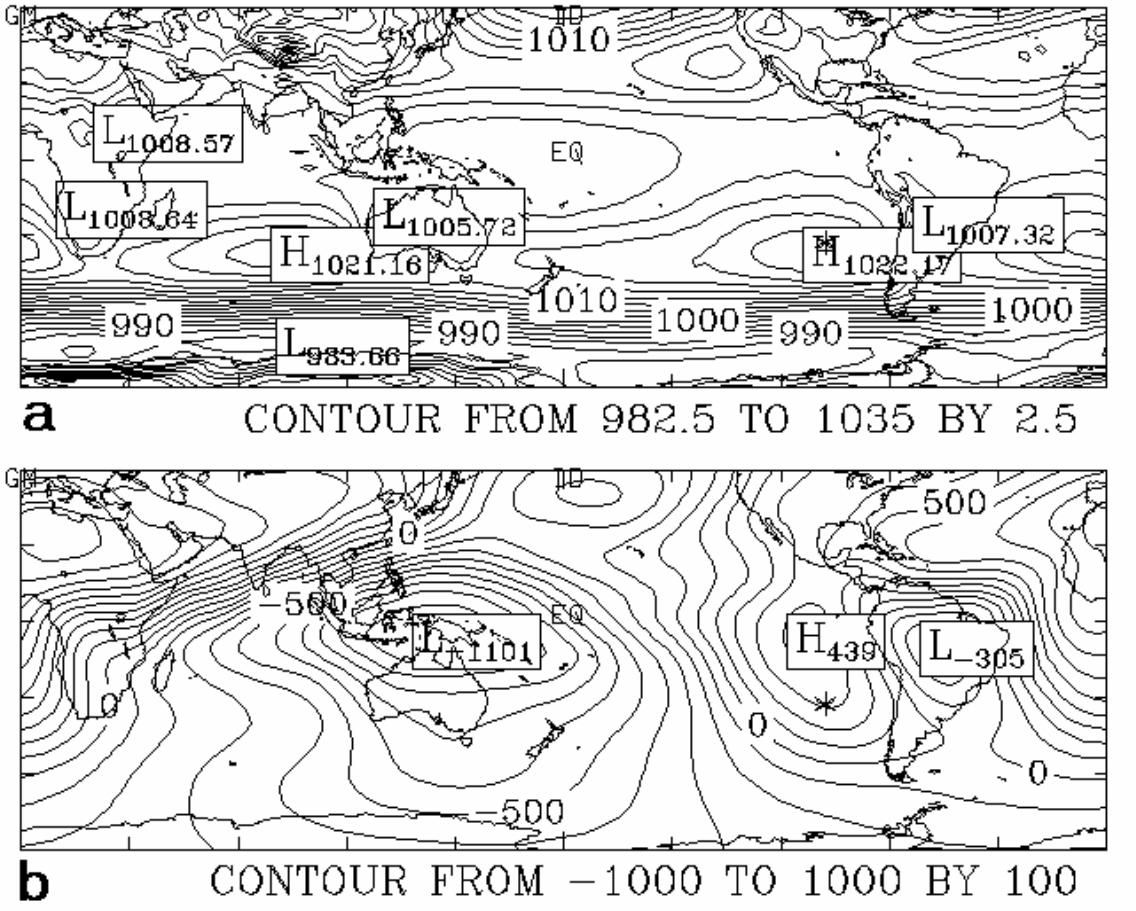

Figure 5. Time mean of: a) daily SLP and b) velocity potential (VP) using all contiguous December, January, and February months from 1979-2002. SLP contour interval is 2.5 hPa. VP contour interval is 10^6 m^2 s^{-1}.

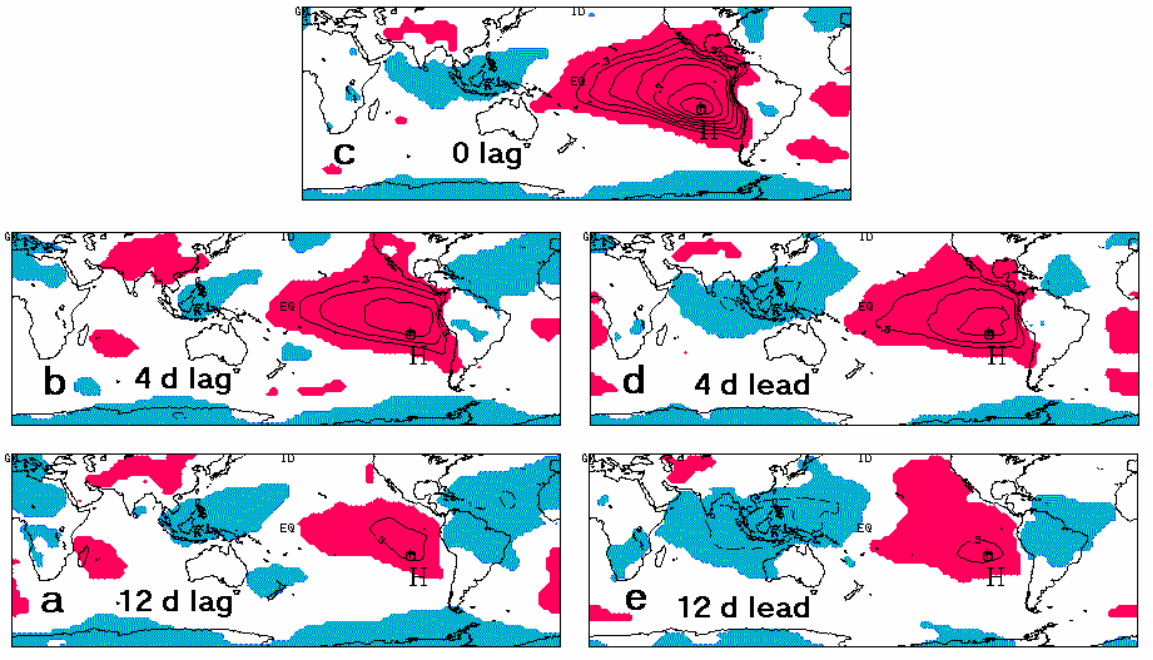

Figure 6. SLP autocorrelations at various lags and lead times for a point (indicated by the circled asterisk) on the north side of the SP high. H marks the location of the time mean SP high center. Correlation contours start at 0.3 with a 0.1 interval. Negative correlations passing both of 2 significance tests at the 1% level have lighter shading with dashed contours; whereas positive correlations are denoted with darker shading and solid contours. In a) the correlation point values lag the two-dimensional field values by 12 days. The timing of the correlations shown is as follows: a) 12 days lag, b) 4 days lag, c) zero lag, d) 4 days lead, e) 12 days lead. Hence, the time evolution of the two dimensional field relative to the correlation point progresses clockwise on these diagrams, starting with a) and ending with e).

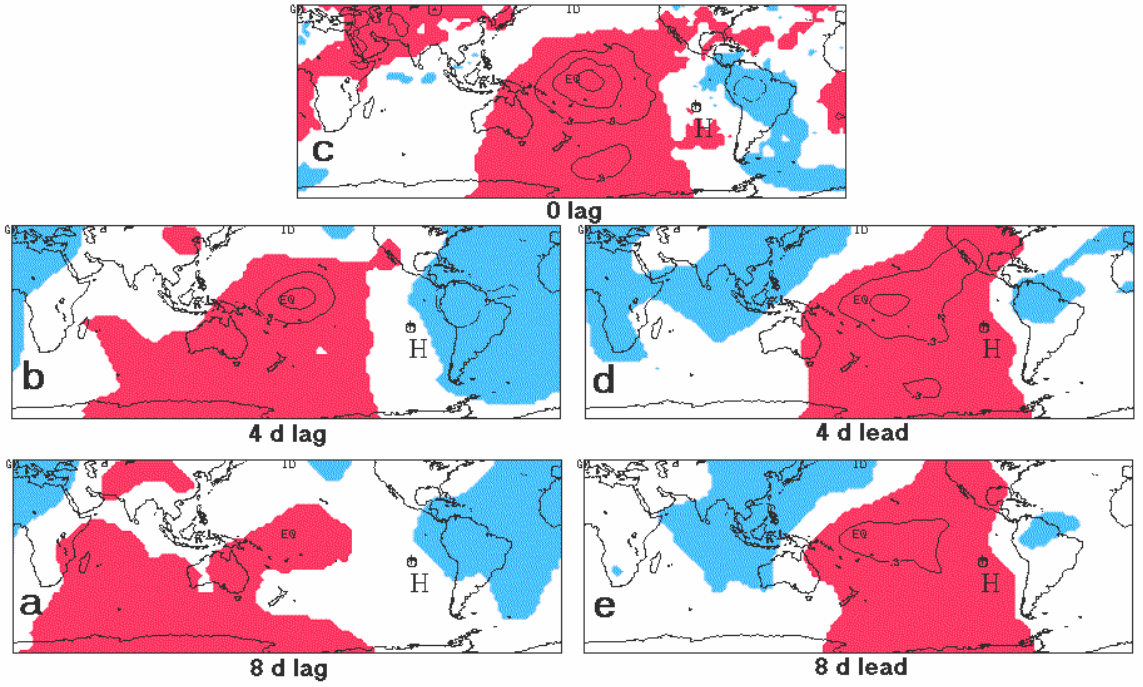

Figure 7. Similar to Figure 6 except for 1-point correlations between SLP at a point and the two dimensional field of VP. The SLP correlation point is on the North side of the SP high and marked by a circled asterisk. H marks the location of the time mean SP high center. Analogous to Figure 6, the time of the VP field progresses clockwise, occurring 8 days before the SLP at the correlation point in a) and proceeding to 8 days after the SLP value in e). Areas of negative significant (at 1% level) correlation have light shading and dashed contours. Darker shading and solid contours denote areas of positive significant correlation. The lowest contour magnitude is 0.3 and a 0.1 interval is used. The times shown are a) 8 days lag, b) 4 days lag, c) zero lag, d) 4 days lead, e) 8 days lead.

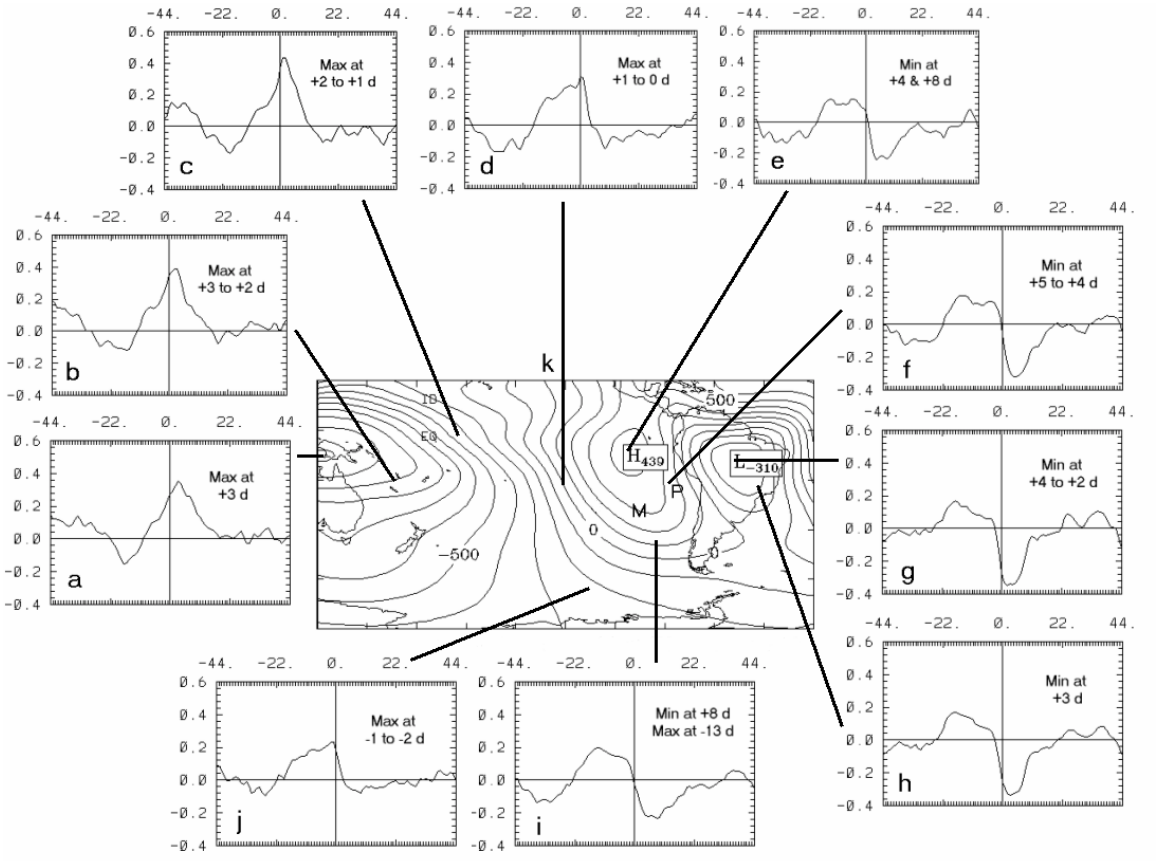

Figure 8. a) – j) Cross-correlation functions between SLP at point "P" and various locations marked on k) the contour plot of VP. "M" marks the location of the maximum in SLP. Point P is on the northeast side of the SP high. VP contour interval is 10^6 m^2 s^{-1}. The cross-correlation diagrams also indicate the timing of the VP maximum or minimum relative to the SLP data. In a) the maximum cross-correlation at the point in Papua New Guinea occurs when the VP data used is 3 days before the corresponding SLP data at point P. See text for discussion.

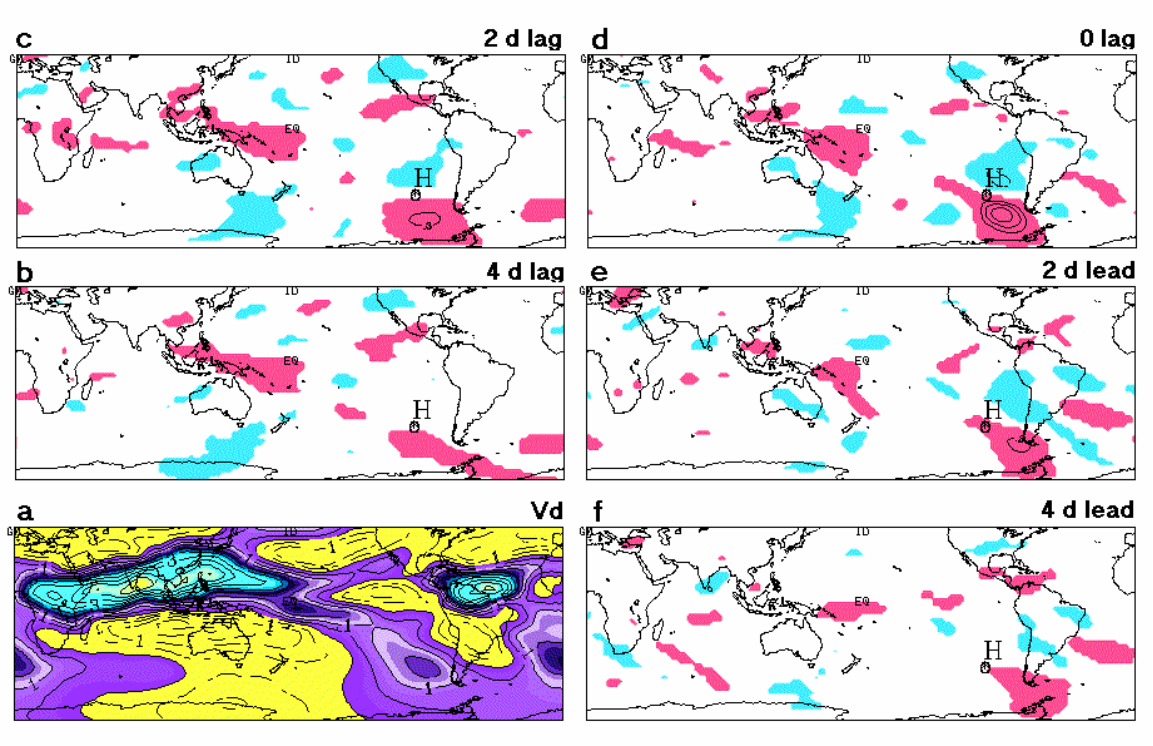

Figure 9. a) Time mean meridional component of divergent wind (Vd) at 200 hPa for all contiguous December, January, and February months during 1979-2002. Northward motion (Vd>0) is contoured using solid lines. Southward motion (Vd<0) is contoured with dashed lines. The contour interval is 0.5 m/s. To better distinguish northward from southward areas, areas of northward motion between 0-2.5 m/s have light or dark shading. b) – f) are similar to Figure 7 except using Vd and a SLP correlation point (indicated by the circled asterisk) on the south side of SP high. Timing of the Vd field relative to the SLP correlation point progresses clockwise from b) to f). In b) the values of Vd are correlated with SLP values 4 days later at the correlation point. The time mean position of the SP high is marked by H. Times shown are b) 4 days lag, c) 2 days lag, d) zero lag, e) 2 days lead, and f) 4 days lead. The south side of the SP high is enhanced by upper level convergence from traveling midlatitude cyclones.

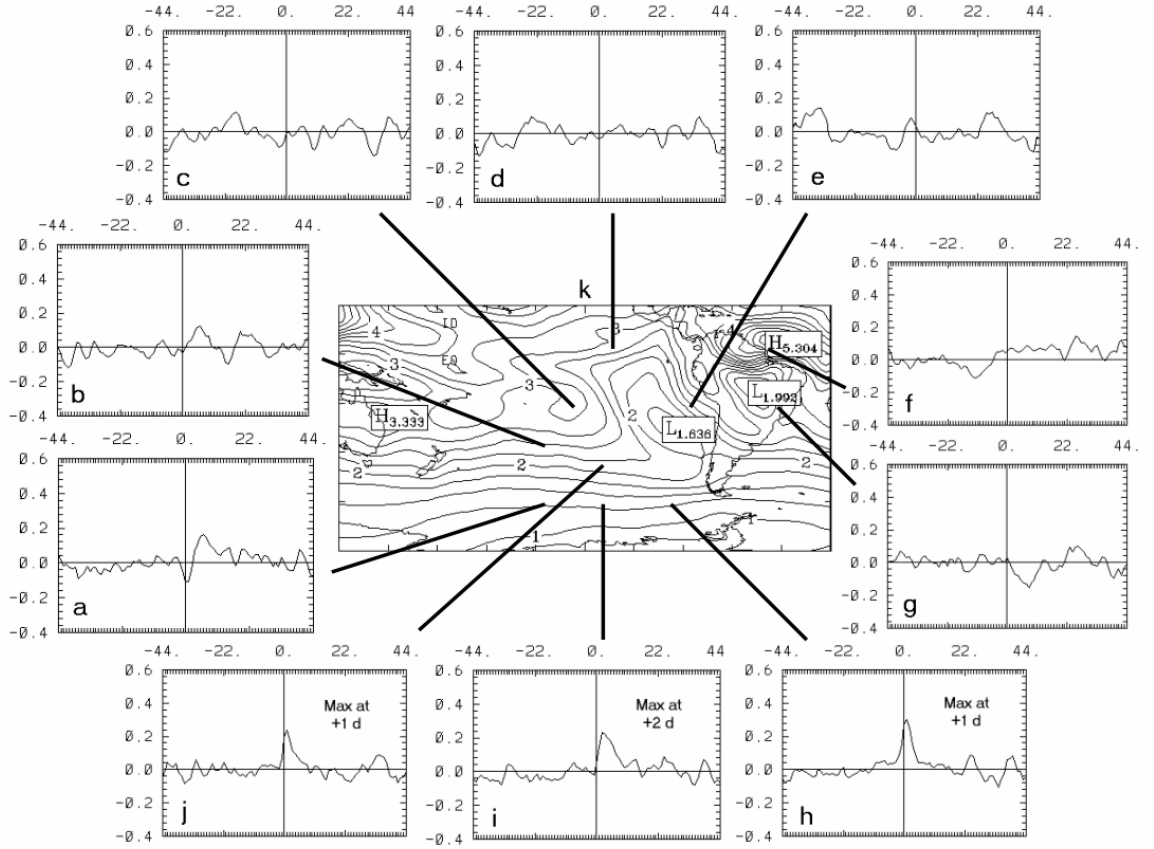

Figure 10. a) – j) Cross-correlation functions between the SLP maximum value and various locations marked on k) the contour plot of divergent wind speed (DWS) at 200 hPa. The DWS contour interval is 1 m/s. The cross-correlation diagrams also indicate the timing of the VP maximum or minimum relative to the SLP data. In i) the maximum cross-correlation at the point in the central South Pacific occurs when the DWS data used are 2 days before the corresponding SLP data. a) – g) do not have cross-correlations exceeding 0.2 in magnitude so no maximum or minimum times are identified. See text for discussion.

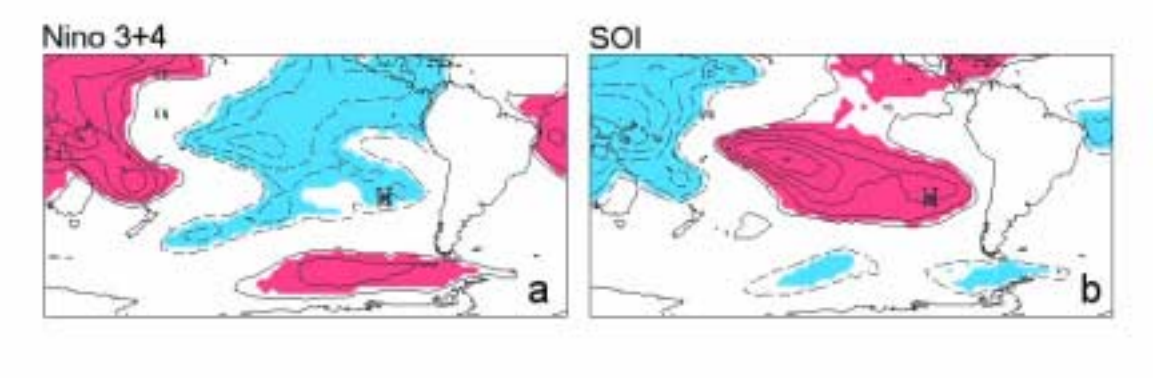

Figure 11: a) Correlation between SLP and an equatorial central Pacific sea surface temperature anomaly index (Nino 3+4). b) Correlation between SLP and the Southern Oscillation Index (SOI). Contours start with magnitude 0.3 and change with 0.1 interval; dashed contours used for negative correlations. Areas of negative correlation passing a pair of 1% significance tests are shaded lightly; darker shading is used for positive significant correlations.